Research Article

Junhong Li*, Ning Cui, Huibin Wu, and Lin He

Dynamic analysis, circuit realization, and its synchronization of a new chaotic hyperjerk system

https://doi.org/10.1515/phys-2025-0171
received January 25, 2025; accepted May 06, 2025

Abstract: This article presents a new chaotic hyperjerk system by adding nonlinear term to an existing model. The dissipativity and invariance, equilibrium points, and their stability conditions, as well as the conditions for the existence of Hopf bifurcations at the equilibrium points, are analyzed. Meanwhile, we investigate the rich dynamical phenomena of the hyperjerk system, and the results show that the system exhibits chaos over a wide range of parameter variations and demonstrates complex dynamical characteristics such as periodic orbits, multi-periodic orbits, and quasi-periodic orbits under different parameter conditions. Furthermore, the chaotic synchronization, and circuit implementation of the hyperjerk system are also studied. Finally, the application of the hyperjerk system in chaotic encryption and decryption is discussed.

Keywords: hyperjerk system, chaos, chaotic synchronization, circuit implementation

1 Introduction

Generally, the study of chaos theory is always based on a specific nonlinear system. Depending on various characteristics, many chaotic systems have been investigated by scholars, such as Duffing systems [1,2], Chen systems [3,4], Genesio systems [5,6], Chua systems [7,8], and Lorenz systems [9,10]. In 2000, Sprott proposed a general form of the jerk system [11], whose general expression is $\dddot{x} = J(\ddot{x}, \dot{x}, x)$, where J is referred to as the jerk function. From physical point of view, x, $\dot{x}$, and $\ddot{x}$ denote the displacement, velocity, and acceleration, respectively. The jerk system has garnered the attention of many researchers due to the simplicity of its equation form and complex dynamical properties. Scholars have presented and studied various versions of the jerk model (see, *e.g.*, [12–14] and references therein). The 4D hyperjerk system can be defined in a form as $x^{(4)} = J(\dddot{x}, \ddot{x}, \dot{x}, x)$, where $x^{(4)}$ can be regarded as "snap" [15]. The hyperjerk system, as an extension of the jerk system, also possesses a simple algebraic structure in its equational expression, yet exhibits more complex dynamical characteristics compared to the jerk system. Vaidyanathan *et al.* [16] presented a new 4D chaotic hyperjerk system having two exponential nonlinearities. The study explored the dissipativity, equilibrium points, stability of the system, as well as its practical circuit implementation and engineering applications. Kaya and Salih [17] analyzed the security of a random number generator based on the 4D the study by Vaidyanathan *et al.* [16]. Jiang *et al.* [18] constructed a new 4D hyperjerk system with antimonotonicity and studied the bifurcations and chaos dynamics of the hyperjerk system. From these, it is evident that the new chaotic model is helpful for a more in-depth exploration of the essence and characteristics of the chaotic system. In addition, due to the high sensitivity of chaos to initial values, it also leads to the difficulty in controlling and predicting chaotic systems. In practical applications, the initial conditions cannot be completely and precisely controlled. Therefore, the research on chaotic synchronization is of great necessity. However, the research on the synchronization phenomenon of the hyperjerk system still needs to be further enriched [19]. Based on the aforementioned reasons, this article further expands the existing models (see previous studies [12,18]) and investigates the complex dynamic characteristics of the new chaotic system and the realization of chaotic synchronization. The circuit implementation of

*** Corresponding author: Junhong Li,** School of Mathematics and Statistics, Hanshan Normal University, Chaozhou, Guangdong, 521041, P. R. China, e-mail: jhli2011@163.com
Ning Cui: School of Mathematics and Statistics, Hanshan Normal University, Chaozhou, Guangdong, 521041, P. R. China
Huibin Wu: School of Mathematics and Statistics, Beijing Institute of Technology, Beijing 100081, China; Beijing Key Laboratory on MCAACI, Beijing Institute of Technology, Beijing 100081, China
Lin He: CSSC Systems Engineering Research Institute, Beijing 100094, China

the new hyperjerk system is also studied. In addition, the application of the new chaotic hyperjerk system in information encryption and decryption was analyzed.

The rest of the article is organized as follows. In Section 2, the dissipativity and invariance, equilibria, and their stability of 4D hyperjerk system are discussed. The complex dynamical behaviors such as the exists of Hopf bifurcation and quasi-periodicity and chaos are also analyzed. The circuit realization, and chaos synchronization are introduced in Section 3 and 4, respectively. The chaotic encryption and decryption using the hyperjerk system are investigated in Section 5. The conclusions are summarized in Section 6.

2 Model and dynamical analysis

A new 4D chaotic hyperjerk system is considered in this article and is described as follows:

$$\begin{cases} \dot{x} = y, \\ \dot{y} = z, \\ \dot{z} = au, \\ \dot{u} = bx - cz - ey - fu - gx^3 - g_0x^2u, \end{cases} \tag{1}$$

where a, c, e, f, g, and g_0 are the positive parameters and $b \in R$. x, y, z, and u are the state variables. The hyperjerk system (1) can be represented as

$$x^{(4)} + (f + g_0x^2)\dddot{x} + ac\ddot{x} + ae\dot{x} + agx^3 - abx = 0.$$

The equation in [18] can be considered as a special case of the hyperjerk model (1) at $b = 1$, $e = 1$, and $g_0 = 0$. The 4D hyperjerk system (1) will be transformed into the 3D jerk system in [12], when $f = g = 1$, $g_0 = 0$, and $y = z$.

2.1 Dissipativity and invariance

It can be seen that system (1) is invariant for the coordinate transformation

$$(x, y, z, u) \to (-x, -y, -z, -u).$$

Thus, the nonzero equilibria of (1) are symmetric with respect to origin. The divergence of the vector field of states of (1) is

$$\nabla V = \frac{\partial \dot{x}}{x} + \frac{\partial \dot{y}}{y} + \frac{\partial \dot{z}}{z} + \frac{\partial \dot{u}}{u} = -f - g_0x^2.$$

Thus, (1) is a dissipative chaotic system.

2.2 Equilibria and their stability

Obviously, (1) always has zero-equilibrium point $P_0 = (0, 0, 0, 0)$, and the characteristic equation of Jacobi matrix at P_0 is

$$f(\lambda) = \lambda^4 + f\lambda^3 + ac\lambda^2 + ae\lambda - ab. \tag{2}$$

When $b < 0$, the real parts of eigenvalues are negative if and only if

$$fc > e, cef + bf^2 > ae^2.$$

P_0 is locally asymptotically stable. When $b > 0$, P_0 is unstable and system (1) has other two nonzero equilibrium points $P_{1,2} = (\pm\sqrt{\frac{b}{g}}, 0, 0, 0)$. The characteristic equation of Jacobi matrix at $P_{1,2}$ is

$$f(\lambda) = \lambda^4 + \left(f + \frac{g_0b}{g}\right)\lambda^3 + ac\lambda^2 + ae\lambda + 2ab. \tag{3}$$

The real parts of eigenvalues are negative if and only if

$$gfc + g_0bc > ge, (fg + bg_0)(aceg - 2bgf - 2g_0b^2) > ag^2e^2$$

[20], then $P_{1,2}$ are locally asymptotically stable. Therefore, for system (1), one has

Theorem 1.

(I) *When* $fc > e, cef + bf^2 > ae^2, b < 0$, *the zero equilibrium point* P_0 *is asymptotically stable. Otherwise, some roots of* (2) *have nonnegative real parts, and* P_0 *is unstable.*

(II) *When* $gfc + g_0bc > ge$, $(fg + bg_0)(aceg - 2bgf - 2g_0b^2) > ag^2e^2$, *and* $b > 0$, *the two nonzero equilibrium points* $P_{1,2}$ *symmetric with respect to the origin are asymptotically stable. Otherwise, some roots of* (3) *have nonnegative real parts, and* $P_{1,2}$ *is unstable.*

2.3 Existence of Hopf bifurcations

Assume that system (1) has a pure imaginary root $\lambda = i\omega$, $(\omega \in \mathbb{R}^+)$. From (2), we obtain

$$\omega^4 - ac\omega^2 - ab = 0, \quad ae - f\omega^2 = 0,$$

then $\omega = \sqrt{\frac{ae}{f}}$, $c = c_* = \frac{ae^2 - bf^2}{afe}$.

Substituting $c = c_*$ into (2), we obtain

$$\lambda_{1,2} = \pm\sqrt{\frac{ae}{f}}\,i, \quad \lambda_{3,4} = \frac{-fe \pm \sqrt{e^2f^2 + 4bef}}{2e},$$

where $ef + 4b > 0, b < 0$. From (2), we have

$$\mathrm{Re}(\lambda'(c_*))|_{\lambda=i\omega} = \frac{a^2e^3f^2}{2(a^2e^4 + 2abe^2f^2 + b^2f^4 - ae^3f^3)} > 0.$$

Thus, the first condition and second condition for a Hopf bifurcation [21] are satisfied. Hence, as c varies and passes through the critical value c_*, (1) undergoes Hopf bifurcations at P_0.

From (3), we obtain

$$\omega = i\sqrt{\frac{aeg}{fg + bg_0}},$$
$$c = c_* = \frac{ae^2g^2 + 2b^3{g_0}^2 + 4b^2fgg_0 + 2bf^2g^2}{a(bg_0 + fg)ge}.$$

Substituting $c = c_*$ into (3), we obtain

$$\lambda_{1,2} = \pm\sqrt{\frac{aeg}{fg + bg_0}}\,i,$$
$$\lambda_{3,4} = \frac{-beg_0 - efg \pm \sqrt{b^2e^2{g_0}^2 + 2be^2fgg_0 + e^2f^2g^2 - 8b^2egg_0 - 8befg^2}}{2eg},$$

where, $beg_0 + fge - 8bg > 0$. Furthermore,

$$\mathrm{Re}(\lambda'(c_*))|_{\lambda=i\omega} = \frac{a^2e^3g^2(g_0b + fg)^2}{2[a^2e^4g^4 - e^2g(g_0b + fg)^2(beg_0 + efg + 4bg)a + 4b^2(g_0b + fg)^4]} > 0.$$

Thus, Hopf bifurcation exists at nonzero-equilibrium point [21,22].

Next, we use the method described in [22] to calculate the first Lyapunov coefficients at P_0 and $P_{1,2}$. When $c = c_*$, the Jacobia matrix at point P_0 and its inverse matrix are

$$A_1 = \begin{bmatrix} 0 & 1 & 0 & 0 \\ 0 & 0 & 1 & 0 \\ 0 & 0 & 0 & a \\ b & -e & -\dfrac{ae^2 - bf^2}{afe} & -f \end{bmatrix},$$

$$A_1^{-1} = \begin{bmatrix} \dfrac{e}{b} & \dfrac{ae^2 - bf^2}{afeb} & \dfrac{f}{ab} & b^{-1} \\ 1 & 0 & 0 & 0 \\ 0 & 1 & 0 & 0 \\ 0 & 0 & a^{-1} & 0 \end{bmatrix}.$$

Through complex calculations, we obtain

$$\eta = \begin{bmatrix} \dfrac{if}{e\sqrt{\frac{ae}{f}}\left(i\sqrt{\frac{ae}{f}}ef^2 - ae^2 - bf^2\right)} \\ -\dfrac{f}{e\left(i\sqrt{\frac{ae}{f}}ef^2 - ae^2 - bf^2\right)} \\ -\dfrac{ia}{\left(i\sqrt{\frac{ae}{f}}ef^2 - ae^2 - bf^2\right)\sqrt{\frac{ae}{f}}} \\ \dfrac{1}{\left(i\sqrt{\frac{ae}{f}}ef^2 - ae^2 - bf^2\right)} \end{bmatrix},$$

$$\xi = \begin{bmatrix} -\dfrac{ibae^2}{2\sqrt{\frac{ae}{f}}} \\ \dfrac{1}{2}ef\left(i\sqrt{\dfrac{ae}{f}}e + b\right) \\ \dfrac{e^2}{2f}\left(iae - f^2\sqrt{\dfrac{ae}{f}}\right)\dfrac{1}{\sqrt{\frac{ae}{f}}} \\ -\dfrac{1}{2}ae^2 \end{bmatrix},$$

which satisfy $A_1\eta = i\omega\eta$, $A_1^T\xi = -i\omega\xi$, and $<\xi, \eta> = 1$. Furthermore, one has the bilinear and trilinear functions in terms of η as

$$B(\eta, \eta) = B(\eta, \bar{\eta}) = \begin{bmatrix} 0 \\ 0 \\ 0 \\ 0 \end{bmatrix},$$

$$C(\eta, \eta, \bar{\eta}) = \begin{bmatrix} 0 \\ 0 \\ 0 \\ -\dfrac{2\left(i\sqrt{\frac{ae}{f}}eg_0 - 3fg\right)\left(iae^2 + ibf^2 - \sqrt{\frac{ae}{f}}ef^2\right)f^3}{a(ae^3f^3 + a^2e^4 + 2abe^2f^2 + b^2f^4)^2\sqrt{\frac{ae}{f}}e^4} \end{bmatrix}.$$

Therefore, the first Lyapunov coefficient at P_0 is

$$l_{10} = \frac{1}{2\omega}\mathrm{Re}(\langle\xi, C(\eta, \eta, \bar{\eta})\rangle) = \frac{f^4\sqrt{\frac{ae}{f}}(3f^3g - ae^2g_0 - bf^2g_0)}{2ae^2(ae^3f^3 + a^2e^4 + 2abe^2f^2 + b^2f^4)^2}.$$

When $c = c_* = \frac{ae^2g^2 + 2b^3{g_0}^2 + 4b^2fgg_0 + 2bf^2g^2}{a(bg_0 + fg)ge}$, the Jacobia matrix at point $P_{1,2}$ and their inverse matrix are

$$A_2 = \begin{bmatrix} 0 & -1 & 0 & 0 \\ 0 & 0 & -1 & 0 \\ 0 & 0 & 0 & -a \\ 2b & e & c_* & \dfrac{bg_0 + fg}{g} \end{bmatrix},$$

$$A_2^{-1} = \begin{bmatrix} \dfrac{e}{2b} & \dfrac{c_*}{2b} & \dfrac{bg_0 + fg}{2gab} & \dfrac{1}{2b} \\ -1 & 0 & 0 & 0 \\ 0 & -1 & 0 & 0 \\ 0 & 0 & -\dfrac{1}{a} & 0 \end{bmatrix}.$$

From $A_2\theta = i\omega\theta$, $A_2^T\zeta = -i\omega\zeta$, and $\langle\zeta, \theta\rangle = 1$, one has

$$\theta = (\theta_{11},\ \theta_{21},\ \theta_{31},\ \theta_{41})^T,$$
$$\zeta = (\zeta_{11},\ \zeta_{21},\ \zeta_{31},\ \zeta_{41})^T,$$

where

$$\theta_{11} = \frac{i(bg_0 + fg)\theta_{41}}{\sqrt{\frac{aeg}{bg_0 + fg}}eg}, \quad \theta_{21} = -\frac{(bg_0 + fg)\theta_{41}}{eg},$$

$$\theta_{31} = \frac{ia\theta_{41}}{\sqrt{\frac{aeg}{bg_0 + fg}}}, \quad \theta_{41} = -\frac{iae^2g(bg_0 + fg) + \sqrt{\frac{aeg}{bg_0 + fg}}\theta_0}{\frac{aeg\theta_0^2}{bg_0 + fg} - a^2e^4g^2(bg_0 + fg)^2},$$

$$\theta_0 = -ae^2g^2 + 2b^3g_0^2 + 4b^2fgg_0 + 2bf^2g^2,$$

$$\zeta_{11} = ibae^2g^2, \quad \zeta_{21} = -\frac{i}{2}eg\sqrt{\frac{aeg}{bg_0 + fg}}\zeta_0,$$

$$\zeta_{31} = \frac{1}{2}\left(i\sqrt{\frac{aeg}{bg_0 + fg}}g + bg_0 + fg\right)e^2g\sqrt{\frac{aeg}{bg_0 + fg}},$$

$$\zeta_{41} = \frac{1}{2}\sqrt{\frac{aeg}{bg_0 + fg}}ae^2g^2,$$

$$\zeta_0 = 2\,ib^2g_0 + 2\,ibfg - \sqrt{\frac{aeg}{bg_0 + fg}}beg_0 - \sqrt{\frac{aeg}{bg_0 + fg}}efg.$$

Therefore, we obtain

$$h_{20} = (2i\omega E - A_2)^{-1}B(\theta, \theta) = \left(0, 0, ah_{20}^*, \left(2\,i\sqrt{\frac{aeg}{bg_0 + fg}} - \frac{bg_0}{g} - f\right)h_{20}^*\right)^T,$$

$$h_{20}^* = -\frac{2\sqrt{\frac{b}{g}}(bg_0 + fg)h_{201}^2\left(3\sqrt{\frac{aeg}{bg_0 + fg}}b^2g_0^2 + 6\sqrt{\frac{aeg}{bg_0 + fg}}bfgg_0 + 3\sqrt{\frac{aeg}{bg_0 + fg}}f^2g^2 + 2\,ig_0ae^2\right)}{gh_{202}^2ae^3\sqrt{\frac{aeg}{bg_0 + fg}}},$$

$$h_{201} = iae^2g(bg_0 + fg) + \sqrt{\frac{aeg}{bg_0 + fg}}(2bf^2g^2 - ae^2g^2 + 2b^3g_0^2 + 4b^2fgg_0),$$

$$h_{202} = \frac{aeg(-ae^2g^2 + 2b^3g_0^2 + 4b^2fgg_0 + 2bf^2g^2)^2}{bg_0 + fg} - a^2e^4g^2(bg_0 + fg)^2,$$

$$h_{11} = -A_2^{-1}B(\theta, \bar{\theta}) = \left(\frac{3\sqrt{\frac{b}{g}}(bg_0 + fg)^4)h_0h_1}{be^4g^2a^2\sqrt{\frac{aeg}{bg_0 + gf}}h_2^2}, 0, 0, 0\right)^T,$$

$$h_0 = i\sqrt{\frac{aeg}{bg_0 + fg}}e(bg_0 + fg)^2 + ae^2g^2 - 2b^3g_0^2 - 4b^2fgg_0 - 2bf^2g^2,$$

$$h_1 = \sqrt{\frac{aeg}{bg_0 + fg}}(2bf^2g^2 - ae^2g^2 + 2b^3g_0^2 + 4b^2fgg_0) + iabe^2gg_0 + iae^2fg^2,$$

$$h_2 = (4b^2f^4 - ae^3f^3 + a^2e^4 - 4abe^2f^2)g^4 + (16b^3f^3g_0 - 3abe^3f^2g_0 - 8ab^2e^2fg_0)g^3$$
$$- (3ab^2e^3fg_0^2 + 4ab^3e^2g_0^2 - 24b^4f^2g_0^2)g^2 + (16b^5fg_0^3 - ab^3e^3g_0^3)g + 4b^6g_0^4,$$

$$C(\theta, \theta, \bar{\theta}) = -\frac{2(bg_0 + fg)^4\left[\sqrt{\frac{aeg}{bg_0 + fg}}(2bf^2g^2 - ae^2g^2 + 2b^3g_0^2 + 4b^2fgg_0) + iabe^2gg_0 + iae^2fg^2\right]^2c_0}{\sqrt{\frac{aeg}{bg_0 + fg}}g^7e^7a^4c_1^3},$$

$$
\begin{aligned}
c_0 = {} & i\sqrt{\frac{aeg}{bg_0+fg}}(ae^3g^2g_0 - 3ae^2g^2 + 6b^3{g_0}^2 + 12b^2fgg_0 \\
& + 6bf^2g^2)(bg_0+fg)^3ae^2g(bg_0+fg) \\
& \times [(3{g_0}^3 - 2g{g_0}^3)b^3 + (9fg{g_0}^2 - 4fg^2{g_0}^2)b^2 \\
& + (9f^2g^2g_0 - 2f^2g^3g_0)b + ae^2g^3g_0 + 3f^3g^3, \\
c_1 = {} & 4b^6{g_0}^4 + 16b^5fg{g_0}^3 + 24b^4f^2g^2{g_0}^2 \\
& + (16f^3g^3g_0 - ae^3g{g_0}^3 - 4ae^2g^2{g_0}^2)b^3 \\
& - (3ae^3fg^2{g_0}^2 + 8ae^2fg^3g_0 - 4f^4g^4)b^2 \\
& - (3ae^3f^2g^3g_0 + 4ae^2f^2g^4)b - ae^3f^3g^4 + a^2e^4g^4.
\end{aligned}
$$

Then, the first Lyapunov coefficient at $P_{1,2}$ is

$$
\begin{aligned}
l_{20} &= \frac{1}{2\omega}\mathrm{Re}[\langle\zeta, C(\theta,\theta,\bar\theta)\rangle - 2\langle\zeta, B(\theta,-h_{11})\rangle + \langle\zeta, B(\bar\theta, h_{20})\rangle] \\
&= \frac{1}{2}e^3g^2a^2(bg_0+fg)^2L_1L_2,
\end{aligned}
$$

where

$$
\begin{aligned}
L_1 = {} & 18f^5g^8 + 90bf^4g^7g_0 + (12bf^4g_0 - 6abe^2f^3g_0 \\
& - 12b^2f^5g_0 + 180b^2f^3{g_0}^2 - 6ae^2f^2g_0)g^6 \\
& + (180b^3f^2{g_0}^3 - 18ab^2e^2f^2{g_0}^2 - 60b^3f^4{g_0}^2 \\
& - 12abe^2fg_0^2 + 48b^2f^3{g_0}^2 - ae^2f^2g_0 \\
& + 2bf^4g_0 + 3f^5)g^5 + (4abe^3f^3{g_0}^2 - 18ab^3e^2fg_0^3 \\
& - 120b^4f^3{g_0}^3 + 8a^2be^4{g_0}^2 - 16ab^2e^2f^2{g_0}^2 \\
& + 90b^4fg_0^4 - 6ab^2e^2{g_0}^3 + 72b^3f^2{g_0}^3 \\
& - 2abe^2fg_0^2 + 8b^2f^3{g_0}^2 + 15bf^4g_0)g^4 \\
& + (12ab^2e^3f^2{g_0}^3 - 6ab^4e^2g_0^4 - 120b^5f^2g_0^4 \\
& - 32ab^3e^2fg_0^3 + 18b^5g_0^5 + 48b^4fg_0^4 - ab^2e^2{g_0}^3 \\
& + 12b^3f^2{g_0}^3 + 30b^2f^3{g_0}^2)g^3 + (12ab^3e^3fg_0^4 - 60b^6fg_0^5 \\
& - 16ab^4e^2g_0^4 + 12b^5g_0^5 + 8b^4fg_0^4 + 30b^3f^2{g_0}^3)g^2 \\
& + (4ab^4e^3g_0^5 - 12b^7g_0^6 + 2b^5g_0^5 + 15b^4fg_0^4)g + 3b^5g_0^5,
\end{aligned}
$$

$$
\begin{aligned}
L_2 = {} & (ae^3f^3 + a^2e^4 - 4abe^2f^2 + 4b^2f^4)g^4 \\
& + (3abe^3f^2g_0 - 8ab^2e^2fg_0 + 16b^3f^3g_0)g^3 \\
& + (3ab^2e^3fg_0^2 - 4ab^3e^2g_0^2 + 24b^4f^2g_0^2)g^2 \\
& + (ab^3e^3{g_0}^3 + 16b^5fg_0^3)g + 4b^6g_0^4.
\end{aligned}
$$

Thus, we derive the following conclusions.

Theorem 2. (*I*) *Suppose* $fe + 4b > 0, b < 0$. *Therefore, when* $l_{10} < 0$ ($l_{10} > 0$), *the Hopf bifurcation is supercritical (subcritical) and a stable (unstable) periodic orbit bifurcating from* P_0 *exists for sufficiently small* $0 < |c - c_*| = |c - \frac{ae^2 - bf^2}{afe}|$.

(*II*) *Suppose* $beg_0 + fge - 8bg > 0, b > 0$. *Therefore, when* $l_{20} < 0$ ($l_{20} > 0$), *the Hopf bifurcation is supercritical (subcritical) and a stable (unstable) periodic orbit bifurcating from* $P_{1,2}$ *exists for sufficiently small* $0 < |c - c_*| = \left|c - \frac{ae^2g^2 + 2b^3{g_0}^2 + 4b^2fgg_0 + 2bf^2g^2}{a(bg_0+fg)ge}\right|$.

Assume

$$a = 10, b = -0.01, f = 10, e = 2, g_0 = 0.01, g = 0.01,$$

then as c varies and passes through the critical value $c_* = 0.205$, (1) undergoes Hopf bifurcations at P_0. A bifurcation periodic solution exists for $c = 0.20499 < c_*$. The corresponding Hopf periodic orbit with $c = 0.20499$ is given in Figure 1. Here, $l_{10} = 7.872 \times 10^{-7} > 0$, then the Hopf bifurcation is subcritical and a unstable periodic orbit bifurcating from P_0.

2.4 Complex dynamical phenomena of hyperjerk system

In this section, some properties of (1) are investigated and the simulation results are further obtained by using numerical methods. In the following, we assume

$$a = 10.5, b = 1.5, c = 1.55, e = 5, f = 100, g = 110.$$

Figure 2 shows that the maximum Lyapunov exponent of system (1) is greater than zero as g_0 varies in [0.5, 100]. Therefore, chaos exists in the hyperjerk system over a large range of parameter variations. when $g_0 = 0.5$, system (1) has unstable node-focus (0, 0, 0, 0) point and unstable saddle-focus points $(\pm\sqrt{\frac{3}{220}}, 0, 0, 0)$. The Lyapunov exponents are 0.04, 0.00, −0.20, and −99.80, Kaplan–Yorke dimension is 2.9984, and the hyperjerk system is chaotic. The chaotic attractors in $x - y$ plane and $z - u$ plane are depicted in Figures 3 and 4, respectively.

The attractors in the 3D spaces (x, y, z), (y, z, u), (x, z, u), and (x, y, u) are shown in Figures 5–8, respectively. The power spectrum of time series $y(t)$ and Poincaré mapping on the $x - y$ plane are given in Figures 9 and 10, respectively. Assume $(b, c, e, g, f, g_0) = (1.5, 1.55, 5, 110, 100, 0.5)$, Figure 11 indicates the bifurcation diagram of variables x, y, z, and u with $a \in [0.5, 15]$. One can see that multi-windows and chaotic attractors can occur as a varies.

Here, multi-period windows of (1) occur when the parameter a varies in the intervals (13.072, 13.71). When $a = 13.2$, the phase diagrams on $x - y$ plane and $z - u$ plane are shown in Figures 12 and 13, respectively.

When

$$(a, b, c, e, f, g, g_0) = (10,1,8.45,10,1,50,10),$$

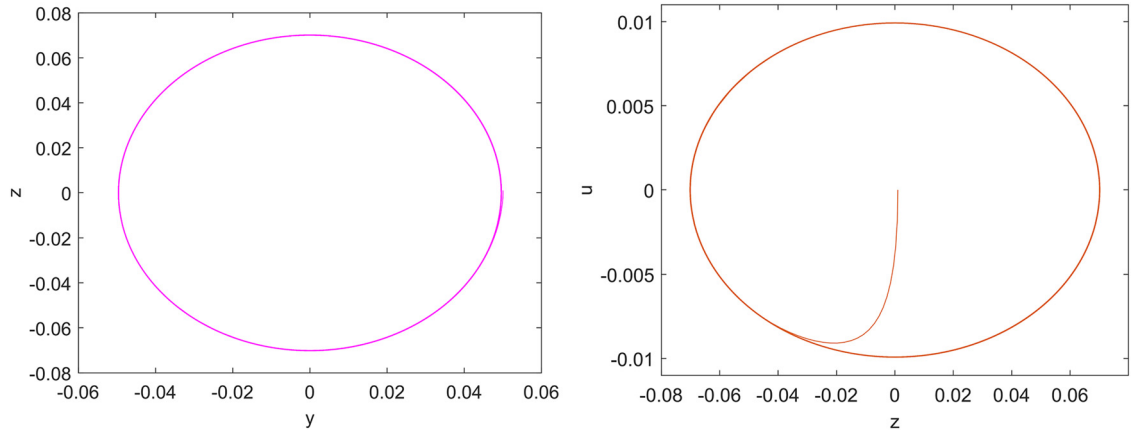

Figure 1: Phase portraits of (1) in $y-z$ plane and $z-u$ plane, respectively.

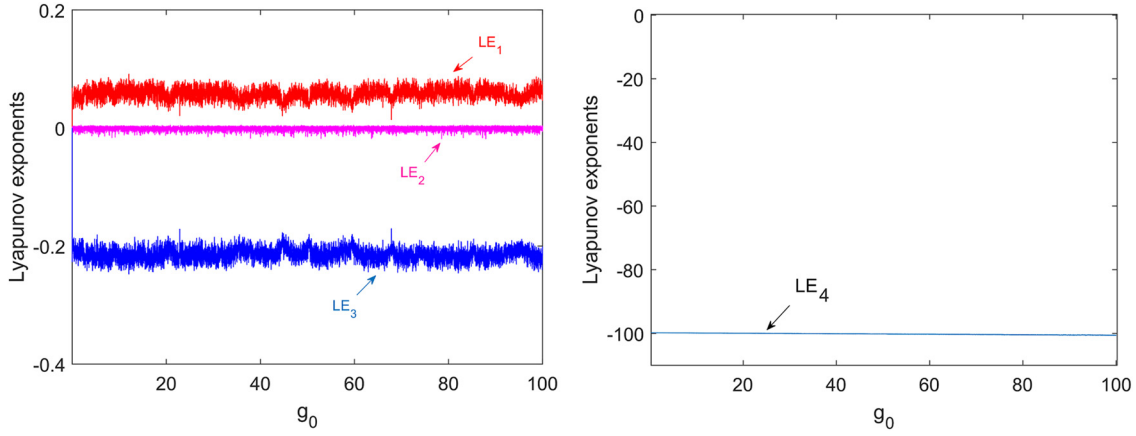

Figure 2: Lyapunov spectrum with the variation of parameter $g_0 \in [0.5, 100]$.

(1) has unstable saddle-focus point $(0, 0, 0, 0)$ and stable node-focus points $(\pm\frac{1}{\sqrt{50}}, 0, 0, 0)$. The Lyapunov exponents are 0.00, 0.00, −0.25, and −0.93; system (1) is quasi-periodic. The corresponding quasi-periodic orbits in $y-z$ plane and $z-u$ plane are shown in Figures 14 and 15, respectively.

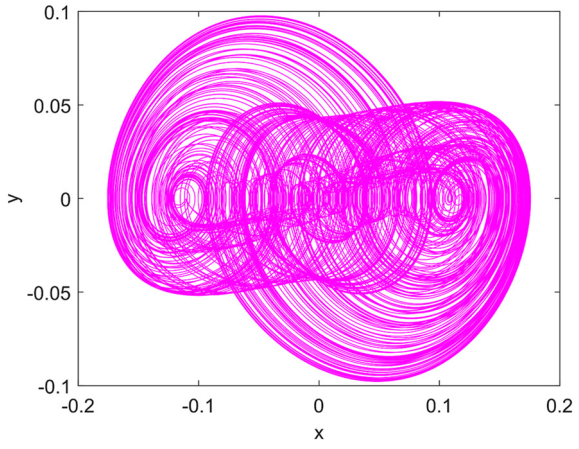

Figure 3: Chaotic attractor of (1) in $x-y$ plane.

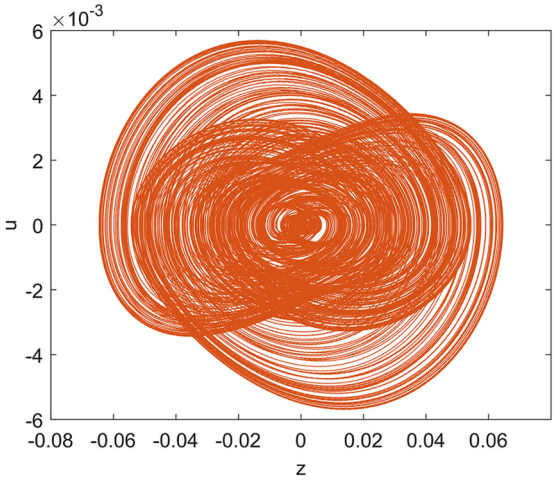

Figure 4: Chaotic attractor of (1) in $z-u$ plane.

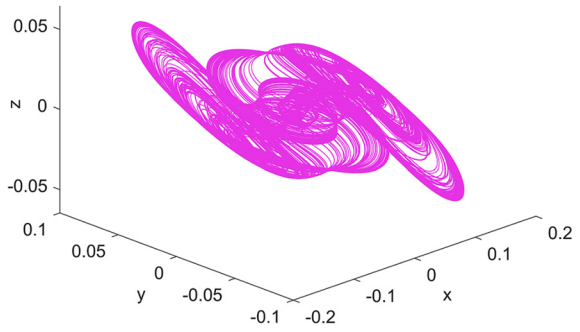

Figure 5: Phase portrait of (1) on $x - y - z$ space.

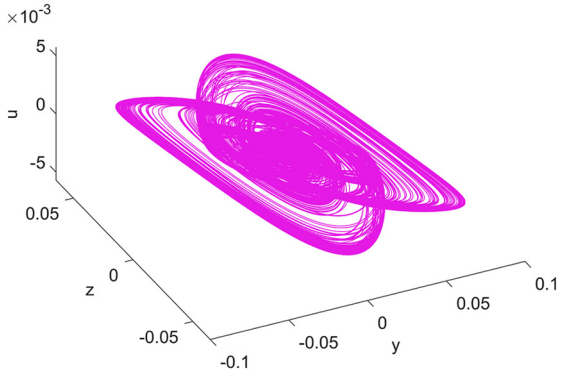

Figure 6: Phase portrait of (1) on $y - z - u$ space.

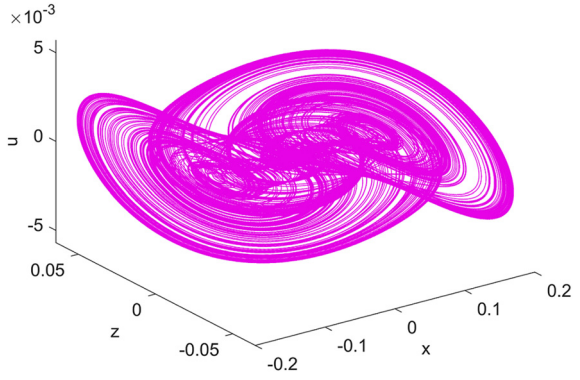

Figure 7: Phase portrait of (1) on $x - z - u$ space.

Overall, it can be seen that the hyperjerk system (1) has rich and complex dynamical characteristics.

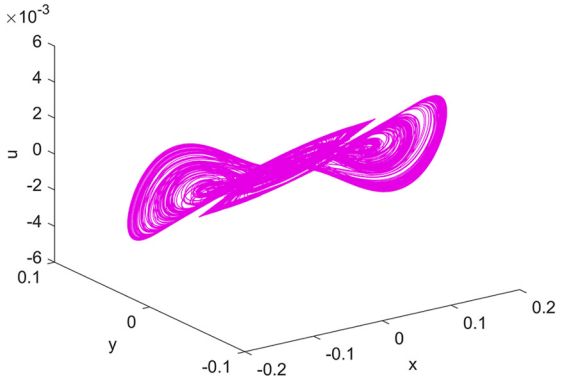

Figure 8: Phase portrait of (1) on $x - y - u$ space.

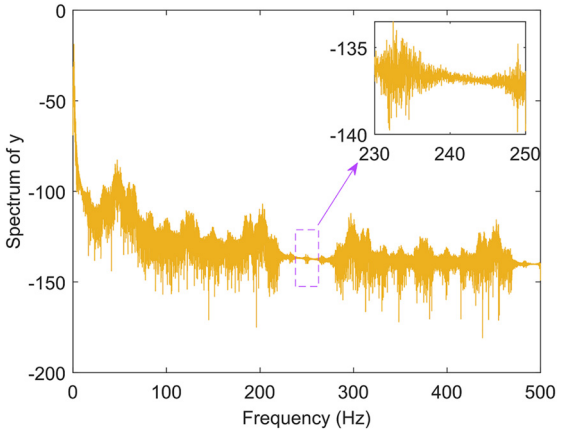

Figure 9: Power spectrum of time series $y(t)$ for (1).

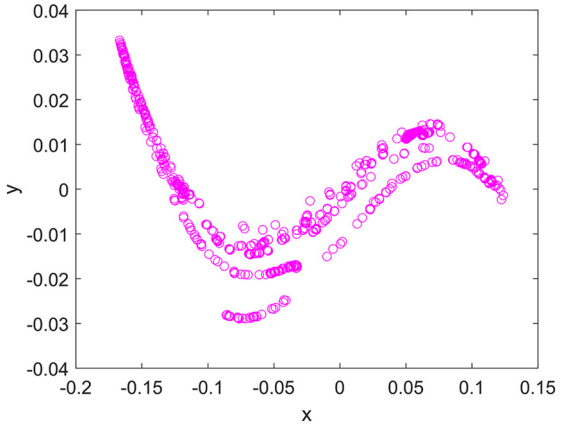

Figure 10: Poincaré mapping on the $x - y$ plane.

3 Chaos synchronization

Since Pecora and Carroll [23,24] first realized experiments on secure communication and information processing using chaotic synchronization, more and more researchers had a thorough research to chaos synchronization [25–27]. In this section, chaos synchronization of the hyperjerk system will be investigated using a nonlinear feedback control. Let the drive system be (1), and the response system is

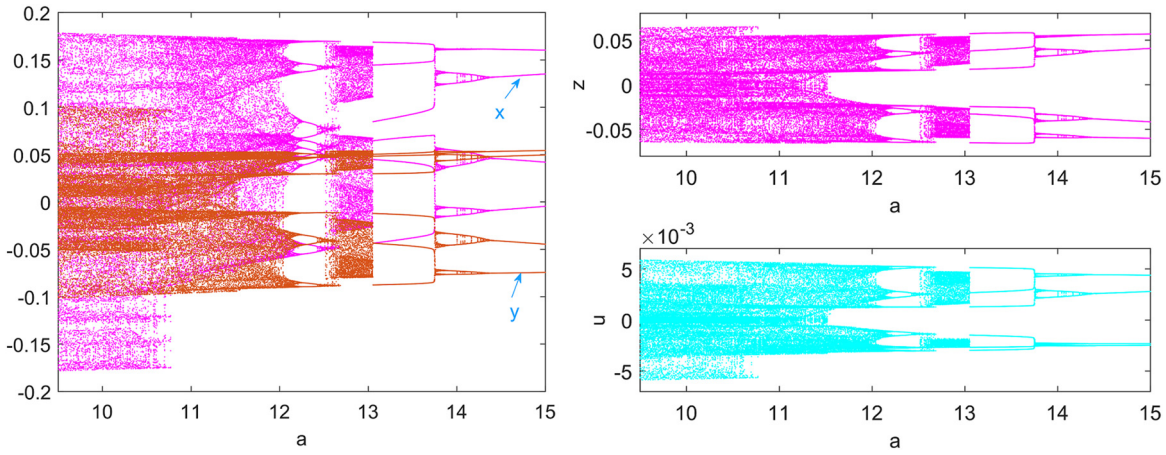

Figure 11: Bifurcation diagram of system (1) with $a \in [0.5, 15]$.

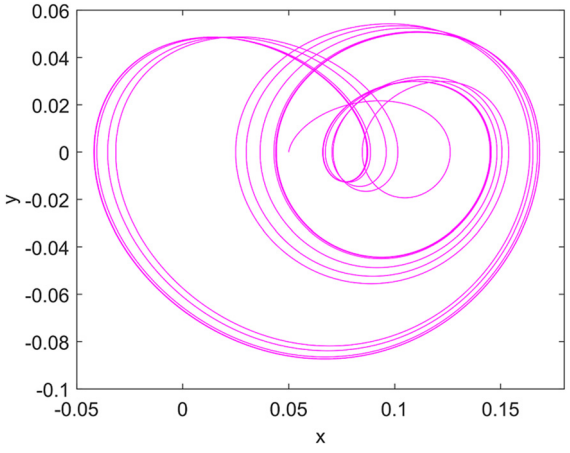

Figure 12: Phase diagram of (1) on $x - y$ plane.

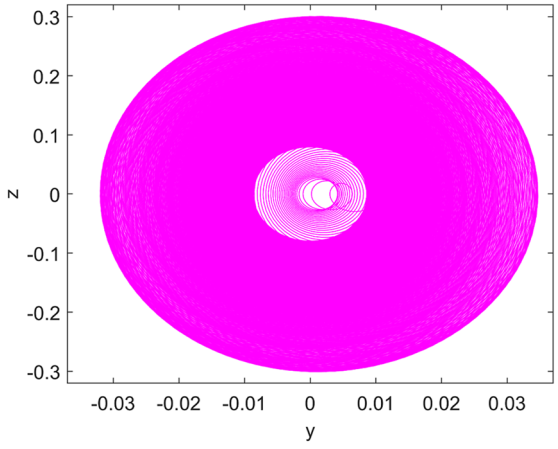

Figure 14: Chaotic attractor of (1) in $x - y$ plane.

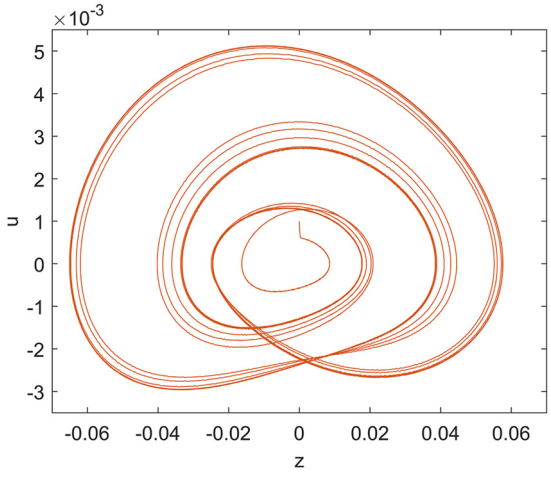

Figure 13: Phase diagram of (1) on $z - u$ plane.

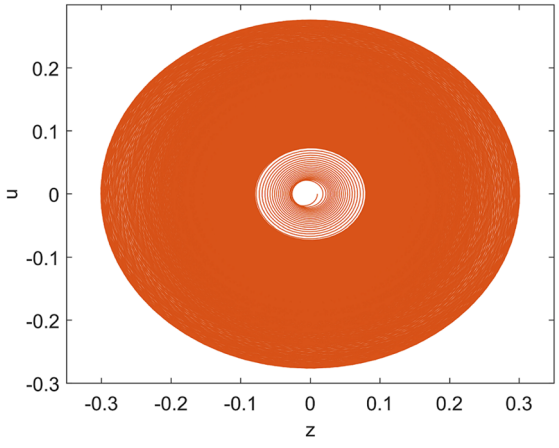

Figure 15: Chaotic attractor of (1) in $z - u$ plane.

$$\begin{cases} \dot{x}_1 = y_1 + \delta_1, \\ \dot{y}_1 = z_1 + \delta_2, \\ \dot{z}_1 = au_1 + \delta_3, \\ \dot{u}_1 = bx_1 - cz_1 - ey_1 - fu_1 - gx_1^3 - g_0x_1^2u_1 + \delta_4, \end{cases} \tag{4}$$

where $(\delta_1, \delta_2, \delta_3, \delta_4)^T$ is the nonlinear controller to be designed. Subtracting system (1) from system (4), we obtain the error equations as follows:

$$\begin{cases} \dot{e}_1 = e_2 + \delta_1, \\ \dot{e}_2 = e_3 + \delta_2, \\ \dot{e}_3 = ae_4 + \delta_3, \\ \dot{e}_4 = be_1 - ce_3 - ee_2 - fe_4 + \delta_0 + \delta_4 \end{cases} \tag{5}$$

where

$$e_1 = x_1 - x, \quad e_2 = y_1 - y, \quad e_3 = z_1 - z, \quad e_4 = u_1 - u,$$
$$\delta_0 = (-e_1^2g_0 + 2e_1g_0x_1 - g_0x_1^2)e_4 - ge_1^3 + (3gx_1 + g_0u_1)e_1^2 + (-3gx_1^2 - 2g_0u_1x_1)e_1.$$

Choose the Lyapunov function $V = \frac{1}{2}\sum_{i=1}^{4} e_i$, the time derivative of V along the trajectory of (5) is

$$\dot{V} = (-e_1^2g_0 + 2e_1g_0x_1 - g_0x_1^2 - f)e_4^2 + (-ge_1^3 + 3ge_1^2x_1 - 3ge_1x_1^2 + g_0u_1e_1^2 - 2g_0u_1x_1e_1 + ae_3 + be_1 - ce_3 - ee_2 + \delta_4)e_4 + \delta_1e_1 + \delta_2e_2 + \delta_3e_3 + e_1e_2 + e_2e_3.$$

Therefore, if we choose δ_i, $(i = 1, 2, 3, 4)$ as follows:

$$\delta_1 = e_1^2e_4g - (3gx_1 + g_0u_1)e_4e_1 - e_1,$$
$$\delta_2 = -ee_4 - e_2,$$
$$\delta_3 = (c - a)e_4 - e_3,$$
$$\delta_4 = -2g_0x_1e_1e_4 - (-3gx_1^2 - 2g_0u_1x_1 + b)e_1,$$

then

$$\dot{V} = -e_1^2e_4^2g_0 - e_4^2g_0x_1^2 - fe_4^2 - e_1^2 + e_1e_2 - e_2^2 + e_2e_3 - e_3^2$$
$$\le -fe_4^2 - e_1^2 + e_1e_2 - e_2^2 + e_2e_3 - e_3^2$$
$$= (e_1, e_2, e_3, e_4)C(e_1, e_2, e_3, e_4)^T,$$

where

$$C = \begin{bmatrix} -1 & \frac{1}{2} & 0 & 0 \\ \frac{1}{2} & -1 & \frac{1}{2} & 0 \\ 0 & \frac{1}{2} & -1 & 0 \\ 0 & 0 & 0 & -f \end{bmatrix}.$$

Obviously, C is negative definite. Hence, the states of drive system (1) and response system (4) are globally synchronized asymptotically. The phase planes of system (4) in $x_1 - y_1$ plane and $z_1 - u_1$ plane are depicted in Figure 16. Dynamics of synchronization errors (e_1, e_2) and (e_3, e_4) for drive system and response system are given in Figures 17 and 18, respectively. From these figures, one can see that the synchronization errors converge to zero and the two systems of (1) and (4) do indeed achieve synchronization of chaos.

4 Circuit realization

From the aforementioned analysis, we can see that the new hyperjerk system can exhibit complex dynamical behaviors. The hardware implementation of theoretical chaotic models is an important topic in practical applications, such as circuit realization [28–30]. This section presents a suitable electronic circuit that emulates the proposed system

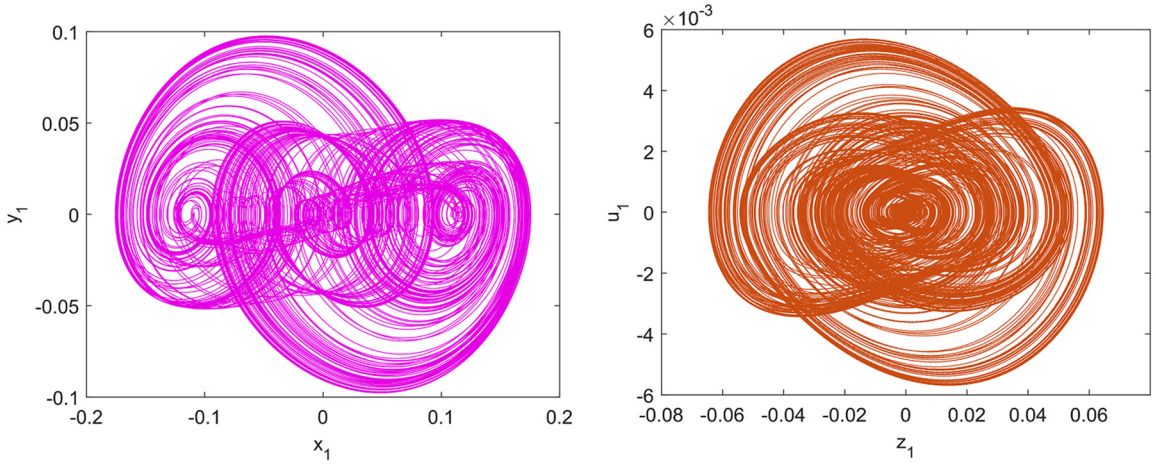

Figure 16: Phase portraits of (4) in $x_1 - y_1$ plane and $z_1 - u_1$ plane, respectively.

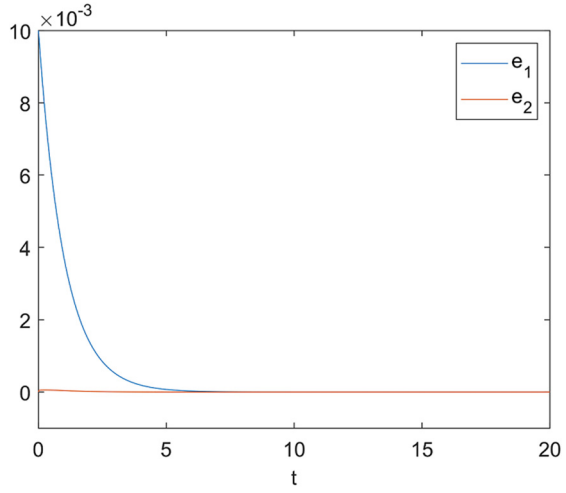

Figure 17: Synchronization errors e_1 and e_2 versus time.

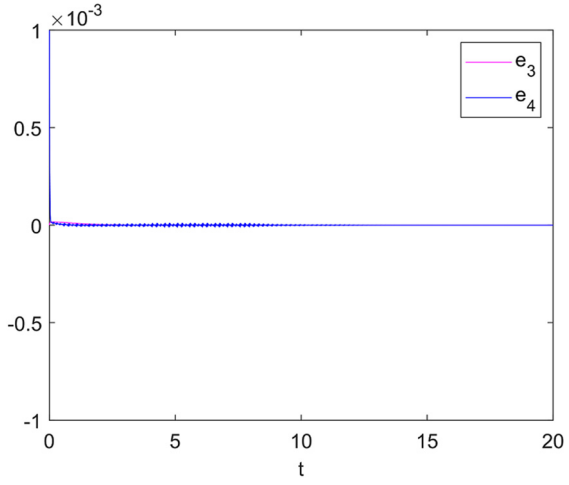

Figure 18: Synchronization errors e_3 and e_4 versus time.

(1). Figure 19 presents the schematic of the circuit that emulates system (1). Here, each of the four channels corresponds to one of the four variables x, y, z, and u, respectively.

The circuit equations are presented as follows:

$$\begin{cases} C_1\dfrac{\mathrm{d}x}{\mathrm{d}\tau} = \dfrac{R_2}{R_1R_3}y, \\ C_2\dfrac{\mathrm{d}y}{\mathrm{d}\tau} = \dfrac{R_7}{R_6R_8}z, \\ C_3\dfrac{\mathrm{d}z}{\mathrm{d}\tau} = \dfrac{R_{12}}{R_{11}R_{13}}u, \\ C_4\dfrac{\mathrm{d}u}{\mathrm{d}\tau} = \dfrac{R_{016}}{R_{22}R_{16}}x - \dfrac{R_{016}R10}{R_{19}R_{16}R_9}y - \dfrac{R_{016}R_{15}}{R_{20}R_{16}R_{14}}z \\ \qquad\qquad - \dfrac{R_{016}R_{24}}{R_{21}R_{16}R_{23}}u - \dfrac{R_{016}R_5}{R_{19}R_{16}R_4}x^3 - \dfrac{R_{016}R_{24}}{R_{18}R_{23}}ux^2, \end{cases} \tag{6}$$

where U_i $(i = 1, 2, \ldots, 12)$ are implemented with the operational amplifier LM675T. The electronic components values have been selected as follows:

$R_1 = R_2 = 50K\Omega$, $R_3 = R_8 = R_{11} = R_{13} = R_{16} = R = 1K\Omega$,
$C_1 = C_2 = C_3 = C_4 = C = 0.1\mu F$,
$R_4 = R_5 = R_6 = R_7 = R_9 = R_{10} = R_{14} = R_{15} = R_{23} = R_{24} = 10K\Omega$,
$R_{12} = 10.5K\Omega$, $R_{20} = 66K\Omega$,
$R_{17} = 0.93K\Omega$, $R_{18} = 204.6K\Omega$,
$R_{19} = 20.46K\Omega$, $R_{21} = 1.023K\Omega$, $R_{22} = 68.2K\Omega$, $R_{016} = 102.3K\Omega$.

The power supplies of all active devices are ±11 V and the experimental time $\tau = RCt$. A_i, $(i = 1, 2, 3, 4)$ are analog multipliers with gain of one. For these chosen components, the system's (1) parameters are as follows:

$$a = 10.5,\ b = 1.5,\ c = 1.55,\ e = 5,\ f = 100,\ g = 110,\ g_0 = 0.5.$$

Figure 20 depicts the experimental observation of circuit's chaotic phenomena in $x - y$ plane (left) and $z - u$ plane (right), respectively. Compared to Figures 3 and 4, one can see that a good agreement between the numerical simulation and the experimental realization is obtained.

5 Chaotic encryption and decryption

Due to the complexity and unpredictability of chaotic systems, chaotic encryption provides a new technical approach for information communication security and has achieved very good results, such as previous studies [29–31]. In this section, taking the sine function as an example, the application of the modified new chaotic hyperjerk system in encryption is illustrated.

Figure 21 indicates the time domain waveforms of the new chaotic hyperjerk system state variables x, y, z, and u. Here, we set the hyperjerk system parameters as $a = 10.5$, $b = 1.5$, $c = 1.55$, $e = 5$, $f = 100$, $g = 110$, $g_0 = 90$, and the initial values as (0.01, 0.01, 0.01, 0.092). During the encryption of the sine sequence, to ensure that the chaotic sequence can mask the plaintext signal and prevent noise from overwhelming or information leakage, the dynamic range of the chaotic sequence used for encryption must cover or modulate the amplitude of the sine sequence. As shown in Figure 21, x has a larger numerical variation range, which facilitates maintaining a uniform distribution when quantizing it into the integer range. Additionally, the higher-order terms in (1) make x more difficult to predict than other variables. Thus, to ensure strong randomness and high security of the chaotic sequence during

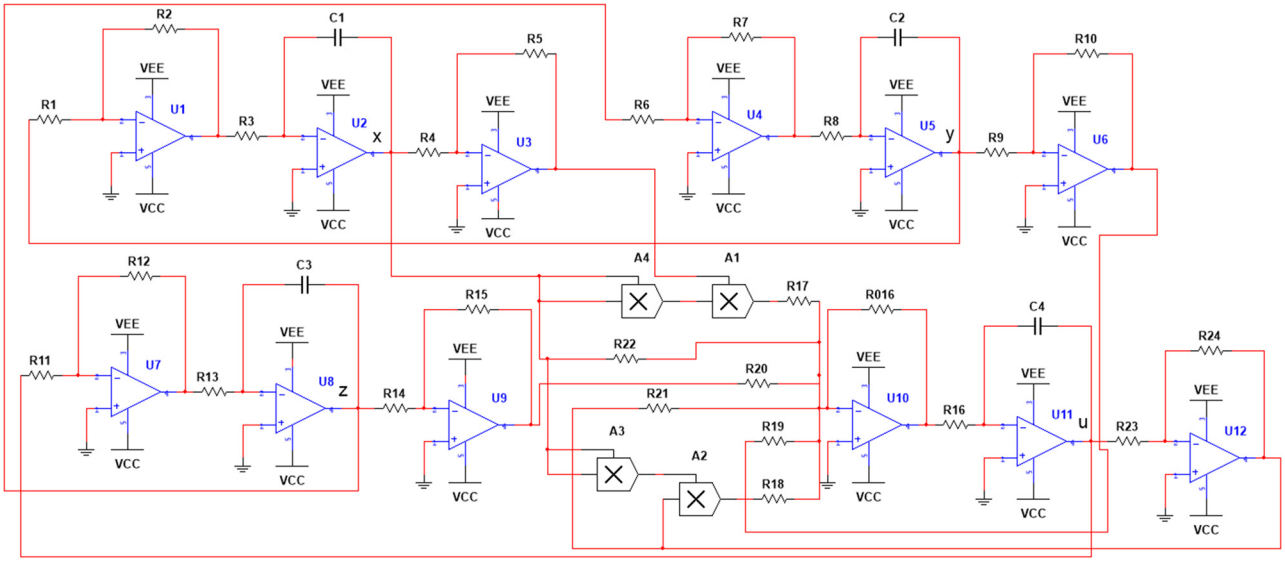

Figure 19: Electronic circuit implementation of 4D hyperjerk system (1).

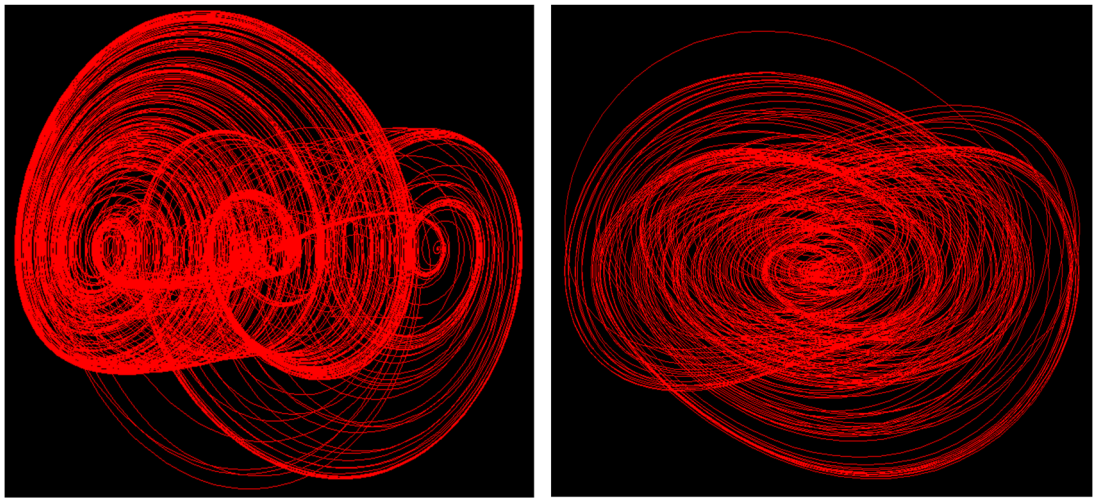

Figure 20: Experimental observation of circuit's chaotic phenomena in different phase portraits.

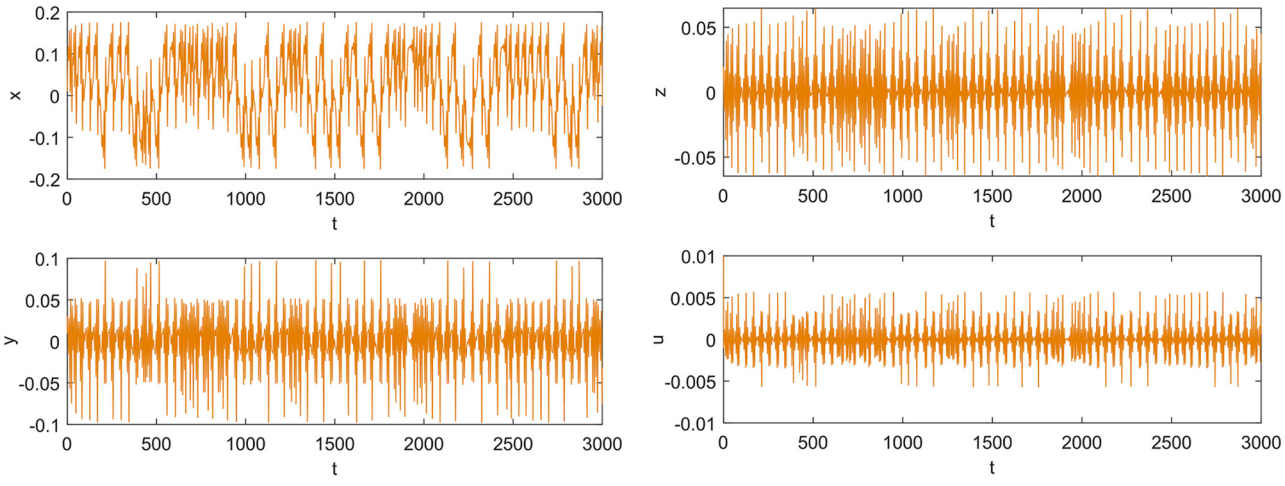

Figure 21: Time domain waveform of the state variables x, y, z, and u.

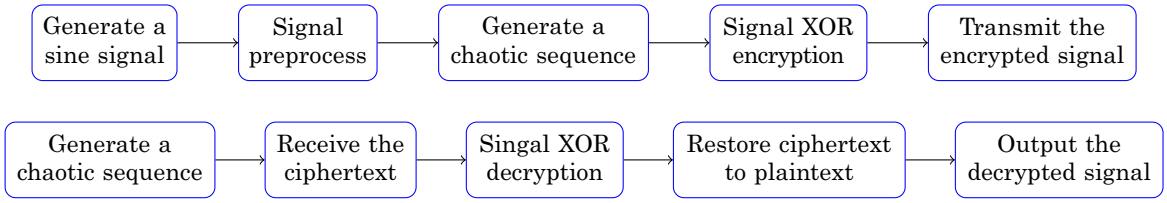

Figure 22: Principle diagram of chaos encryption and decryption.

encryption, we select the chaotic sequence generated by the state variable x for encrypting the sine sequence. Figure 22 shows the principles of encryption and decryption using the new chaotic hyperjerk system (1). The first row is using chaos to encrypt the sine signal. The specific encryption process is as follows: (I) a sine sequence is generated as the plaintext to be encrypted using the equation $S = \sin(2\pi ht)$, where the time $t \in [0, 1]$, the sequence length is 3,000, and the sine wave frequency $h = 10$ Hz; (II) normalize the sine signal from $[-1, 1]$ to $[0, 255]$, and the mapping equation is $S_1 = \text{round}((S + 1) \times 127.5)$; (III) the new chaotic hyperjerk system is discretized using the fourth-order Runge–Kutta method, and x is extracted as the signal for encryption. Furthermore, the chaotic sequence $C = \text{mod}([|x \times 10^5|], 256)$ is generated. Here, we select the same parameter values and initial conditions as those in Figure 21; (IV) both S_1 and C are converted to the unit8 type, and then the sine sequence is encrypted through the XOR encryption algorithm $C \oplus S_1$ to generate the ciphertext S_E; (V) transmit the ciphertext. The second row is using chaos for decryption. The specific decryption process is as follows: (P1) generate a chaotic sequence C_d identical to that in (III); (P2) receive the ciphertext S_E; (P3) decrypt S_E using the XOR algorithm $C_d \oplus S_E$ to obtain the signal sequence D_E; (P4) use the inverse mapping to obtain the plaintext $S_D = \frac{D_E}{127.5} - 1$; (P5) output the decrypted signal sequence S_D. The effect of chaotic encryption and decryption using the hyperjerk system is shown in Figure 23. It can be seen that the encrypted chaotic sequence effectively conceals the original sequence data, and the decrypted sequence is highly consistent with the original sequence.

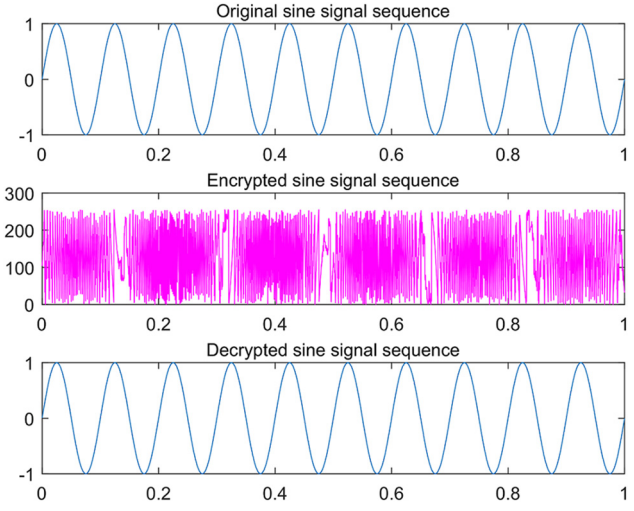

Figure 23: Chaotic encryption and decryption using the hyperjerk system.

6 Conclusions

Based on the model in Jiang *et al.* [18], this article reports a new chaotic hyperjerk system by adding nonlinear term. The models in Jiang *et al.* [18] and Elsonbaty *et al.* [12] can be seen as special cases of the proposed model. The results of the study show that the system is a dissipative system symmetric with respect to the origin. When $b < 0$, the system has only one zero equilibrium point; when $b > 0$, the system exhibits two nonzero equilibrium points, which are symmetric about the origin. Hopf bifurcations occur at these equilibrium points under certain conditions. Simulation results indicate that the system exhibits various complex dynamical phenomena under different parameter conditions, including periodic orbits, multi-periodic orbits, quasi-periodic orbits, and chaotic attractors. This article not only generalizes the models in existing references and discovers new complex dynamical phenomena, but also achieves chaotic synchronization by selecting appropriate nonlinear controllers and realizes the chaotic hyperjerk system using electronic components. Moreover, it explores the practical application of the new hyperjerk system in chaotic encryption and decryption, with good results.

Acknowledgments: The project was supported by the University Characteristic Innovation Project of Guangdong Province (No. 2023KTSCX079) and by the Doctoral Scientific Research Foundation of Hanshan Normal University (No. QD202130).

Funding information: The authors state no funding involved.

Author contributions: Junhong Li – original draft; Ning Cui – review and editing; Huibin Wu and Lin He – supervision. All authors have accepted responsibility for the entire content of this manuscript and approved its submission.

Conflict of interest: The authors state no conflict of interest.

Data availability statement: All data generated or analyzed during this study are included in this published article.

References

[1] Lei Y, Huan M, Du L. Onset of colored-noise-induced chaos in the generalized Duffing system. Nonlinear Dynam. 2017;89(2):1371–83.

[2] Ouannas A, Khennaoui AA, Momani SM, Pham VT. The discrete fractional duffing system: chaos, 0-1 test, C complexity, entropy, and control. Chaos. 2020;30(8):083131.

[3] Liu X, Shen X, Zhang H. Multi-scroll chaotic and hyperchaotic attractors generated from chen system. Int J Bifurcat Chaos. 2012;22(02):1250033.

[4] Rech PC. Chaos suppression instigated by a hyperbolic sine nonlinearity in the Chen system. Int J Mod Phys C. 2021;32(10):2150133.

[5] Zhou L, Chen F. Hopf bifurcation and Sialnikov chaos of Genesio system. Chaos Soliton Fract. 2009;40(3):1413–22.

[6] Dogan N. Numerical solution of chaotic Genesio system with multi-step Laplace Adomian decomposition method. Kuwait J Sci. 2013;40(1):109–21.

[7] Stegemann C, Albuquerque HA, Rubinger RM, Rech PC. Lyapunov exponent diagrams of a 4-dimensional Chua system. Chaos. 2011;21(3):033105.

[8] Alvarez-Ramirez J, Rodriguez E, Echeverria JC, Puebla H. Correlation analysis of chaotic trajectories from Chuaas system. Chaos Soliton Fract. 2008;36(5):1157–69.

[9] Luo C, Wang X. Chaos in the fractional-order complex Lorenz system and its synchronization. Nonlinear Dynam. 2013;71(1):241–57.

[10] Naveen S, Parthiban V. Existence, uniqueness and error analysis of variable-order fractional Lorenz system with various type of delays. Int J Bifurcat Chaos. 2024;34(12):2450152.

[11] Sprott JC. A new class of chaotic circuit. Phys Lett A. 2000;266(1):19–23.

[12] Elsonbaty AR, El-Sayed AA. Further nonlinear dynamical analysis of simple jerk system with multiple attractors. Nonlinear Dynam. 2017;87(2):1169–86.

[13] Kengne LK, Muni SS, Chedjou CK. Various coexisting attractors, asymmetry analysis and multistability control in a 3D memristive jerk system. Eur Phys J Plus. 2022;137(7):848–61.

[14] Chen Y. Codimension-2 bifurcations of a generalized three-dimensional cubic jerk system. Computat Appl Math. 2024;43:169.

[15] Chlouverakis KE, Sprott JC. Chaotic hyperjerk systems. Chaos Soliton Fract. 2006;28(3):739–46.

[16] Vaidyanathan S, Akgul A, Kacar AS, Çavuşoğlu U. A new 4-D chaotic hyperjerk system, its synchronization, circuit design and applications in RNG, image encryption and chaos-based steganography. Eur Phys J Plus. 2018;133:46.

[17] Kaya D, Salih E. Security analysis of a random number generator based on a chaotic hyperjerk system. EPL. 2020;129(3):30001.

[18] Jiang L, Li J, Zhang W. Bifurcations and chaos dynamics of a hyperjerk system with antimonotonicity. Eur Phys J Plus. 2020;135:767.

[19] Ernesto Z, Andres A. A novel antimonotic hyperjerk system: analysis, synchronization and circuit design. Phys D. 2021;424:132927.

[20] Edmund XD, Charles K. Routh-Hurwitz criterion in the examination of eigenvalues of a system of nonlinear ordinary differential equations. Phys Rev A. 1987;35(12):5288–90.

[21] Guckenheimer J, Holmes P. Nonlinear oscillations, dynamical systems and bifurcations of vector fields. New York: Springer; 1983.

[22] Kuznetsov YA. Elements of applied bifurcation theory, 2nd edn. New York: Springer-Verlag; 1997.

[23] Pecora L M, Carroll TL. Synchronization in chaotic systems. Phys Rev Lett. 1990;64:821–7.

[24] Carroll TL, Pecora LM. Synchronization chaotic circuits. IEEE Trans Circ Syst. 1991;38(4):453–6.

[25] Aghababa MP, Heydari A. Chaos synchronization between two different chaotic systems with uncertainties, external disturbances, unknown parameters and input nonlinearities. Appl Math Model. 2012;36(4):1639–52.

[26] Yang N, Yang S, Wu C. A novel fractional-order chaotic system and its synchronization circuit realization. Mod Phys Lett B. 2022;36(23):2250114.

[27] Yan S, Wang J, Li L. Analysis of a new three-dimensional jerk chaotic system with transient chaos and its adaptive backstepping synchronous control. Integration. 2024;98:102210.

[28] Biswas D, Banerjee T. A simple chaotic and hyperchaotic time-delay system: design and electronic circuit implementation. Nonlinear Dynam. 2016;83(4):2331–47.

[29] Cai X, Liu C, Wang Y, Zhang H. A novel 4D chaotic system with nonhyperbolic hyperbolic shape equilibrium points: analysis, circuit implementation and color image encryption. Int J Mod Phys B. 2020;33(31):1950383.

[30] Zhang J, Liu E, Rubio A. Circuit design and image encryption of CNN chaotic system based on memristor. Eur Phys J B. 2024;97(7):100.

[31] Liu Y, Fang F, Liu J. Chaotic systems based secure communication scheme for detection of wind turbines. IEEE T Smart Grid. 2023;14(6):4704–16.